ACS APPLIED MATERIALS & INTERFACES

Research Article

www.acsami.org

Design of a Sorbent to Enhance Reactive Adsorption of Hydrogen Sulfide

Long-Jiang Wang,[†] Hui-Ling Fan,*[,†] Ju Shangguan,[†] Eric Croiset,[‡] Zhongwei Chen,[‡] Hui Wang,[§] and Jie Mi[†]

[†]State Key Laboratory of Coal Science and Technology, Co-founded by Shanxi Province and the Ministry of Science and Technology, Institute for Chemical Engineering of Coal, Taiyuan University of Technology, West Yingze Street Number 79, Taiyuan 030024, People's Republic of China

[‡]Department of Chemical Engineering, University of Waterloo, 200 University Avenue West, Waterloo, Ontario N2L 3G1, Canada

[§]Department of Chemical Engineering, University of Saskatchewan, Saskatoon, Saskatchewan S7N 5A9, Canada

Supporting Information

ABSTRACT: A series of novel zinc oxide−silica composites with three-dimensionally ordered macropores (3DOM) structure were synthesized via colloidal crystal template method and used as sorbents for hydrogen sulfide (H_2S) removal at room temperature for the first time. The performances of the prepared sorbents were evaluated by dynamic breakthrough testing. The materials were characterized before and after adsorption using scanning electron microscopy (SEM), transmission electron microscopy (TEM), nitrogen adsorption, X-ray diffraction (XRD), Fourier transform infrared (FTIR) spectroscopy and X-ray photoelectron spectroscopy (XPS). It was found that the composite with 3DOM structure exhibited remarkable desulfurization performance at room temperature and the enhancement of reactive adsorption of hydrogen sulfide was attributed to the unique structure features of 3DOM composites; high surface areas, nanocrystalline ZnO and the well-ordered interconnected macroporous with abundant mesopores. The introduction of silica could be conducive to support the 3DOM structure and the high dispersion of zinc oxide. Moisture in the H_2S stream plays a crucial role in the removal process. The effects of Zn/Si ratio and the calcination temperature of 3DOM composites on H_2S removal were studied. It demonstrated that the highest content of ZnO could reach up to 73 wt % and the optimum calcination temperature was 500 °C. The multiple adsorption/regeneration cycles showed that the 3DOM ZnO−SiO_2 sorbent is stable and the sulfur capacity can still reach 67.4% of that of the fresh sorbent at the fifth cycle. These results indicate that 3DOM ZnO−SiO_2 composites will be a promising sorbent for H_2S removal at room temperature.

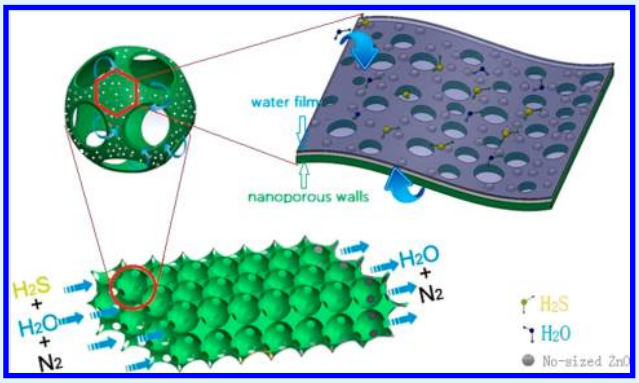

KEYWORDS: *zinc oxide−silica composites, 3DOM structures, moisture, H_2S adsorption, room temperature*

1. INTRODUCTION

Hydrogen sulfide, as a major impurity, is present in natural gas, syngas, biogas and other industrial gases.[1−3] The impurity is necessary to be removed to less than a few ppmv because it is highly harmful to both technological processes and the environment.[4] For example, hydrogen sulfide at levels as low as 3 ppm can bring about severe pipeline corrosion.[5] Catalysts used in the fuel processing units (FPUs) and electrolytes of fuel cells (FCs) will be poisoned even if FC reformates contain <1 ppmv of sulfur.[6,7] Furthermore, hydrogen sulfide can convert to SO_2 during combustion, which is also corrosive and causes acid rain.[8] With increasingly environmental regulations, the emission of sulfur compounds is limited greatly.[9] Therefore, searching for various materials with excellent desulfurization performance is urgent and very meaningful.

ZnO, as an important sorbent for removal of H_2S, has attracted great attention due to the favorable thermodynamics of its sulfidization reaction, its thermal stability and its nonpyrophoric property.[10−12] Zinc oxide reacts with hydrogen sulfide to form the insoluble zinc sulfide via the reaction:

$$ZnO(s) + H_2S(g) \Leftrightarrow ZnS(s) + H_2O(g)$$

$$\Delta G = -91607.18 + 15.16T\ (J\ mol^{-1})^{12}$$

As this reaction is exothermic, a lower temperature favors the forward reaction, resulting in high efficiency of desulfurization. However, the rate of reaction is reduced at lower temperatures.

Received: September 6, 2014
Accepted: November 10, 2014
Published: November 10, 2014

Therefore, development of a ZnO sorbent that can rapidly remove H_2S at room temperature has been the focus of studies on desulfurization for the past few years.[4,13−19]

Stirling et al.[20] showed in a study that the zinc oxides prepared through the coprecipitation route had higher surface areas than those of their impregnated counterparts and thus had greater capacity for H_2S removal at low temperatures. They also found that the reaction of the cobalt−zinc mixed oxides with H_2S is largely confined to the surface of the oxides.[21] A high surface area is a property of the materials that is essential to their function as adsorbents. Carnes and Klabunde[22] studied the H_2S adsorption on nanocrystalline metal oxides of Zn, Ca, Mg and Al at low temperatures (25−100 °C) and compared it with that on commercially available microcrystalline metal oxides. They found that the yield of sulfidation of nanocrystalline ZnO (4 nm) is 13 times that of a commercial ZnO (44 nm). Nanocrystalline ZnO is expected to compensate the slower sulfidation kinetics at low temperatures by enhancing the reactivity with H_2S due to its quantum size effects and high surface/volume ratio.[12,23]

In recent years, supported ZnO low-temperature H_2S sorbents have been investigated mainly because they benefit from high surface area and nanocrystalline ZnO. Numerous studies[18,19,23] have been concentrated on ZnO supported on mesoporous silicas, such as MCM-41, KIT-6, SBA-15, MSU-1 and SiO_2. ZnO supported on activated carbon has also been reported.[24] However, the sulfur capacities of sorbents obtained in these studies are limited because of the drawbacks of active phase loading; excessive loading can result in insufficient dispersion of metal oxides and partial clogging of pores.[18] Davidson and co-workers.[25−27] considered that sorbent reactivity was more strongly dependent upon porosity than upon the surface, as sulfidation between ZnO and H_2S may cause pore blocking due to the greater molar volume of ZnS (V_{solid} = 2.4 × 10^{-5} m^3/mol) than that of zinc oxide (V_{solid} =1.45 × 10^{-5} m^3/mol). A study by Ilaria Rosso et al.[28] showed that internal mass-transfer resistance at low temperature limited the sulfidation rate of ZnO sorbent; increasing the internal open porosity of the sorbent by exploiting a multimodal pore distribution with macro- and micropores could improve its performance. Montes et al.[19] and Liu et al.[18] reached similar conclusions that the adsorption capacity of the obtained materials at room temperature strongly depends on the pore system.

It can be summarized that a desirable ZnO sorbent should have the maximum amount of active components while remaining a high surface area, good dispersion as well as an advanced porosity.

Three-dimensionally ordered macroporous (3DOM) materials consist of a very ordered skeleton surrounding uniform, close-packed macropores interconnected through windows. Such materials are very porous, and their specific surface areas are high because their structures inhibit agglomeration of active species and favor nanosized grains. Such materials have attracted considerable attention because of their potential applications in technologies such as electrochemical sensors, separation, photonic crystals and heterogeneous catalysis.[29−32]

Thus, 3DOM materials combine most of the characteristics that are required by an ideal ZnO-based sorbent for use at ambient temperature. Furthermore, 3DOM iron-oxides prepared in our previous study exhibited unexpected good results and proved the great potential of their structure in desulfurization at medium temperatures.[33] This encouraged us to explore a zinc oxide sorbent with 3DOM structure and to use it for sulfur removal at ambient temperature. In this work, 3DOM ZnO/SiO_2 composites were synthesized for the first time by the colloidal crystal templating method and their performance in H_2S adsorption was evaluated.

2. EXPERIMENTAL SECTION

2.1. Chemicals. Zinc nitrate hexahydrate (AR, 99%), tetraethylorthosilicate (reagent grade, 98%), potassium persulfate (AR, 99.5%), methanol (AR, 99.5%), ethylene glycol (AR, 98%) and ethanol absolute (GR, 99.8%) were purchased from Aladdin Chemistry Co. Ltd. Polyvinylpyrrolidone (AR, K27-32) and styrene (AR, 98%) were obtained from Tianjin Damao Chemical reagent Factory. Hydrochloric acid (AR, 99.5%) was purchased from Guangzhou Chemical reagent Factory. All the chemicals were used without further purification.

2.2. Sorbent Preparation. 3DOM materials were prepared by colloidal crystal template method. The synthesis of monodispersed polystyrene (PS) microspheres and assembly of PS colloidal crystal templates are described elsewhere in detail.[33] For preparation of 3DOM composites, the typical procedures are as mentioned below. First, silica sol was prepared by mixing tetraethylorthosilicate (TEOS), anhydrous ethanol (EtOH), hydrochloric acid and distilled water at a molar ratio of 1:3.9:0.3:1.8. Then zinc nitrate hexahydrate was dissolved in a mixture of ethylene glycol (EG) and methanol (the final concentration of methanol was 40 vol %) to achieve the zinc nitrate solution (1.5 M). After that, certain amounts of silica sol and zinc nitrate solution were mixed to get the final precursor solution with different Zn content. The PS hard templates were then immersed in the above precursor solution for 16 h. Excess solution was removed from the impregnated templates by vacuum filtration. The obtained product was dried at room temperature overnight, and then calcined under flowing air in a muffle furnace to remove the PS template. The temperature was first raised from 30 to 300 °C at a heating ramp of 1 °C min^{-1} and kept at this temperature for 2 h, then increased to 500 °C at the same ramp and held for 4 h. In this work, 3DOM materials with the weight ratios of ZnO of 20%, 50% and 73% were obtained, and were named as 3D-SZx-500 in which x denotes the ZnO weight ratio in percent. In addition, the 3DOM materials with 50 wt % ZnO calcined at different temperature ranged from 400 to 700 °C for 4h were also prepared. The final products were named as 3D-SZ50-y, where y indicates the calcination temperature. The used 3DOM material for H_2S capture was named as 3D-SZx-yE. In view of convenient for comparison, 3DOM SiO_2 was prepared using silica sol as precursor solution and was named as 3D-SiO_2, silica sol and the final precursors of the mixture of silica sol and zinc nitrate solution were directly calcined using the same drying and calcinating process as 3D-SZx-500 to get silica and silica-zinc oxide composites without 3DOM structure which was named as SZ-50-500. A commercial desulfurizer (HTZM-1) containing 60% ZnO, which is applied at ambient temperature in industry, was provided by Liaoning Haitai Scientific and Technological Development Co., Ltd. for comparison. The name of HTZM-1 is shorten to be CZ.

2.3. Characterization of Materials. Nitrogen adsorption−desorption isotherms were measured using a Micromeritics 3H-2000PS2 instrument. The BET surface areas were calculated by the standard Brunauer−Emmett−Teller method. Micropore surface areas and micropore volumes were determined by t-plot method. The Barrett−Joyner−Halenda (BJH) modal was employed to calculate the pore size distributions (PSDs) and the total pore volumes from the desorption branches of the isotherms. Powder X-ray diffraction (XRD) patterns were obtained on Rigaku D/max-2500 diffractometer with Cu Kα radiation. The Fourier transform infrared (FTIR) spectra were performed on a 670 FT-IR spectrophotometer (Thermo Nicolet, USA) (400−4000 cm^{-1}). X-ray photoelectron spectroscopy (XPS) measurements were made on a V.G. Scientific ESCALAB250 spectrometer. Scanning electron microscopy (SEM) and high-resolution transmission electron microscopy (HRTEM) images were taken using Nanosem430 and Tecnai G2 F20 electron microscopy, respectively.

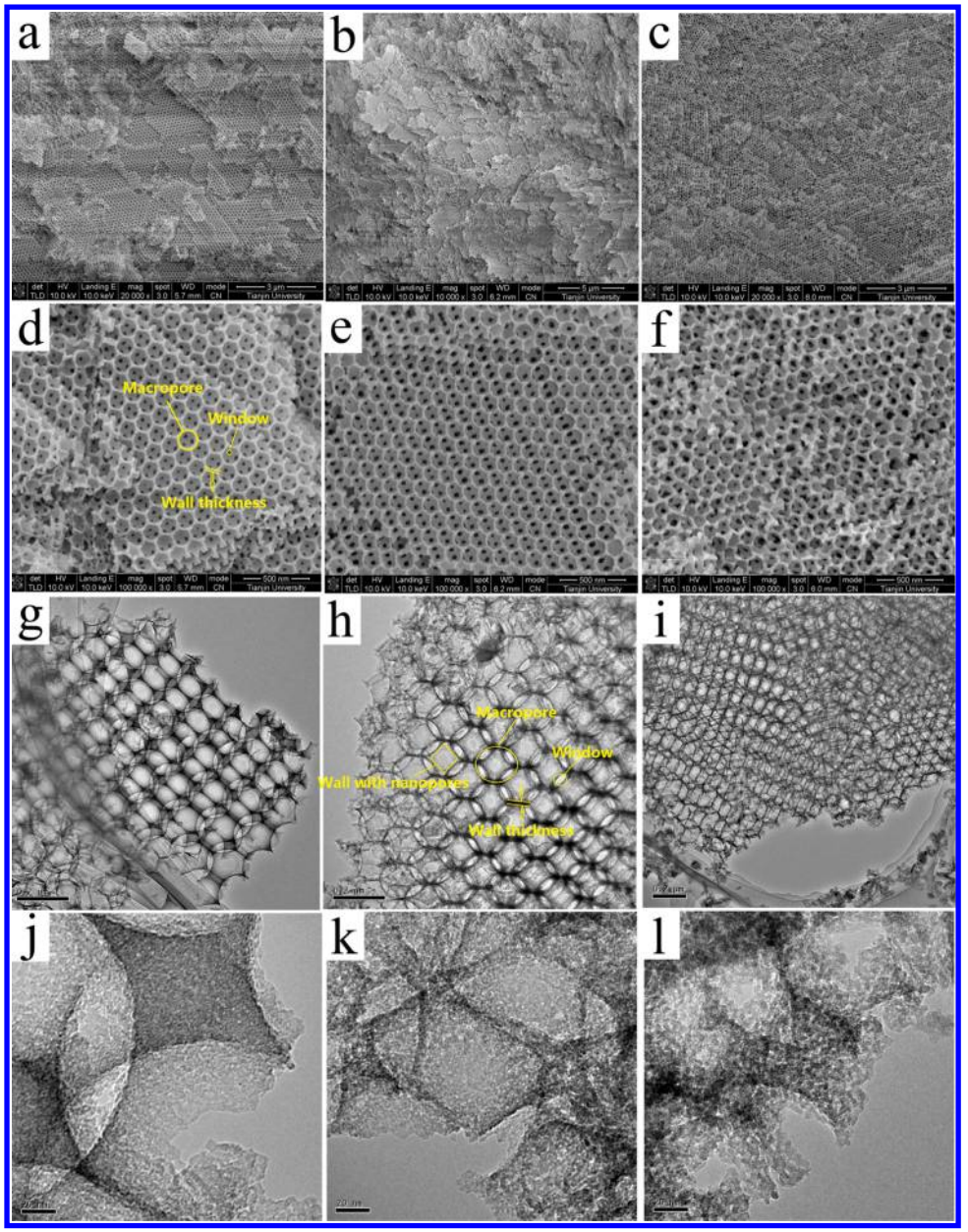

Figure 1. SEM (a–f) and TEM (g–l) images, at different magnifications, of the prepared 3DOM composites: 3D-SZ20-500 (a, d, g, j); 3D-SZ50-500 (b, e, h, k); 3D-SZ73-500 (c, f, i, l). (a–c) Large area view of the materials.

2.4. Performance Tests. The typical dynamic tests were carried out to determine the breakthrough capacities of the adsorbents for H_2S removal under moisture atmosphere. The adsorbents were crushed into particles of 60–80 mesh and packed into a glass reactor with inner diameter of 6 mm and a bed height used was 2 cm. Before the tests, the adsorbents in bed were prehumidified with the moist N_2 (ca. 3% moisture) which was obtained by passing a flow of N_2 through a bubbler controlled at room temperature. After that, moist N_2 (ca. 3% moisture) containing 500 mg/m^3 was passed through the column of the sorbent at a flow rate of 100 mL/min. The concentrations of H_2S in outlet were monitored using a gas chromatograph (Haixin, GC-920) equipped with a photometric detector (FPD). In this work, the breakthrough concentration of H_2S was defined as 1 mg/m^3 and the breakthrough sulfur capacity is defined as milligrams of sulfur per gram of material at the breakthrough point.

3. RESULTS AND DISCUSSION

3.1. Morphology and Porous Structure. Figure 1 shows SEM and TEM images of 3D-SZx-500 samples. It can be seen that well-ordered three-dimensional macroporous strucutures were obtained in high yields. Large fractions of the samples had the 3DOM structure spanning tens of micrometers, resembling a honeycomb. The macropore size of 3D-SZx-500 was about ~120 nm, indicating ~40% shrinkage relative to the initial size of PS microspheres (200 nm, Figure S1, Supporting Information). This shrinkage was due to melting of polymer templates and sintering of the produced oxides.[33] Macropores were interconnected in three dimensions through small windows of ~30 nm in diameter. The walls of macropores were about 15 nm in thicknesses and the magnified TEM images (j, k, l) further show the existence of mesopores within the walls. These mesopores are considered to be formed due to the aggregation of ultrafine nanocrystallized particles.[34] The

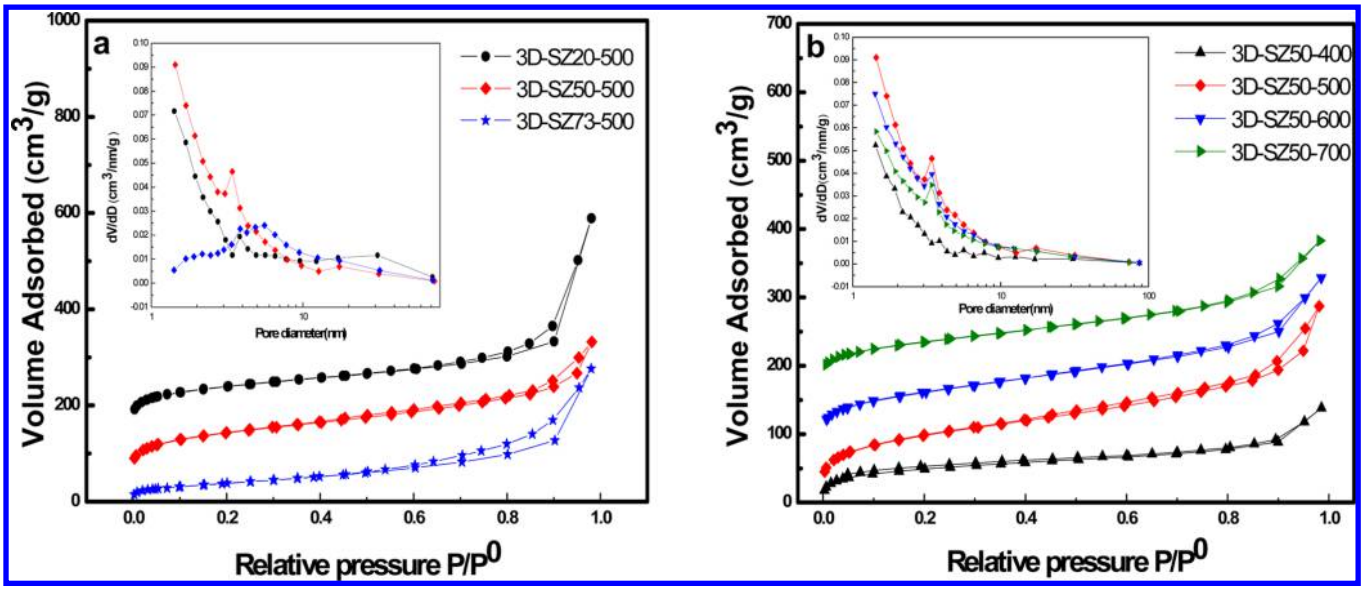

Figure 2. Nitrogen adsorption−desorption isotherms of fresh samples (a, b). Insert: pore size distributions calculated by BJH method.

morphology and structure of the 3D-SZ50-y samples were similar to those of 3D-SZ50-500, and the 3DOM structure was retained even at calcination temperatures of 700 °C (Figure S2, Supporting Information). The structure ordering of 3D-SZ73-500 decreased and the 3DOM structure deviated from ideality. Furthermore, the structure was difficult to obtain through the procedure when the ZnO content increased to 80%. Evidently, a sufficient amount of silica was required to support the three-dimensional macroporous structure. This indicates that silica can stabilize the 3DOM structure.

Figure 2 shows the nitrogen adsorption−desorption isotherms and pore size distribution obtained through the BJH method. It can be seen that all of the 3D-SZ samples produced a type II isotherm according to the IUPAC classification, and nitrogen adsorption markedly increased at a relative pressure above 0.8, characteristic of a macroporous structure.[29,35] A type H3 hysteresis loop formed in the relative pressure (p/p^0) range of 0.8−1.0, indicating that 3D-SZ samples possessed a mesoporous structure,[36] which can be observed in the TEM images. Moreover, the inflection point for all 3D-SZ samples except 3D-SZ73-500 emerged at relative pressures below 0.1. This implies the existence of a small number of micropores.[37] The corresponding pore size distributions (PSDs) show that the mesopore sizes were dominantly distributed between 3.0 and 4.0 nm and that some pore sizes were distributed within 10−70 nm. In the case of 3D-SZ73-500, mesopore sizes were broadly distributed (3−10 nm) and almost no micropores were present.

Texture parameters of all samples are listed in Table 1. For the 3D-SZx-500 samples, the surface areas and total pore volumes decreased with the increase in Zn/Si ratio, indicating that high ZnO content resulted in a reduction of the surface area and pore volume. Furthermore, the BET surface areas and pore volumes of the 3D-SZ50-y samples (except 3D-SZ50-400) decreased gradually at higher calcination temperature. These changes occurred mainly because the channels shrunk slowly with the calcination temperature increasing, as proven by the corresponding PSDs. In the case of 3D-SZ50-400, the black appearance, rather than the gray-white of the other samples, suggests carbon impurities remained because of insufficient calcination, which was further confirmed by energy dispersive

Table 1. Textural Parameters of the 3D-SZ Composites[a]

sample	S_{BET} (m^2/g)	S_{mi} (m^2/g)	V_{mi} (cm^3/g)	V_t (cm^3/g)	W_{BJH} (nm)
3D-SZ20-500	357	132	0.055	0.70	1.416
3D-SZ50-500	336	74	0.029	0.44	1.436
3D-SZ73-500	142	0	0	0.43	5.572
3D-SZ50-400	266	146	0.062	0.25	1.423
3D-SZ50-500	336	74	0.029	0.44	1.436
3D-SZ50-600	293	60	0.026	0.38	1.417
3D-SZ50-700	235	43	0.018	0.33	1.402
3D-SZ50-500E	174	134	0.056	0.34	1.410

[a] S_{BET}, BET specific area; S_{mi}, micropore area; V_{mi}, micropore volume; V_t, total pore volume; W_{BJH}, pore size determined from BJH desorption data.

X-ray (EDX) analysis. These carbon impurities can lead to partial blockage of pores and a decrease in surface area.[38]

Thus, the prepared composites have a well-ordered and interconnected pore network with hierarchically porous consisting of macro-, meso-, and micropores, as well as a high surface area mainly due to micro- and mesopores. The Zn/Si ratio and calcination temperature played a major role in dictating the properties of the 3DOM structure.

3.2. XRD Analysis. Figure 3 shows X-ray diffraction patterns of the fresh and sulfided samples. It can be seen from Figure 3a that all samples showed a typical amorphous structure except 3D-SZ73-500, which gave obvious diffraction peaks corresponding to ZnO. However, the peaks of 3D-SZ20-500 and 3D-SZ50-500 at ~25° shifted slightly toward angles larger than those corresponding to SiO_2.[18,39] This shift might be due to introduction of ZnO and good dispersion of ZnO in the 3DOM composites. Moreover, a shoulder at ca. 30° and a large band at ca. 60°, corresponding to the characteristic reflection of the ZnO phase, emerged in the patterns of 3D-SZ50-500, indicating that formation of very small ZnO nanoparticles.[40] These results are revealed by the TEM images (see Figure 1, j−l). The intensity of the shoulder and band of the 3D-SZ50-y samples (Figure 3b) increased slowly with calcination temperature, suggesting that the nanoparticles grew

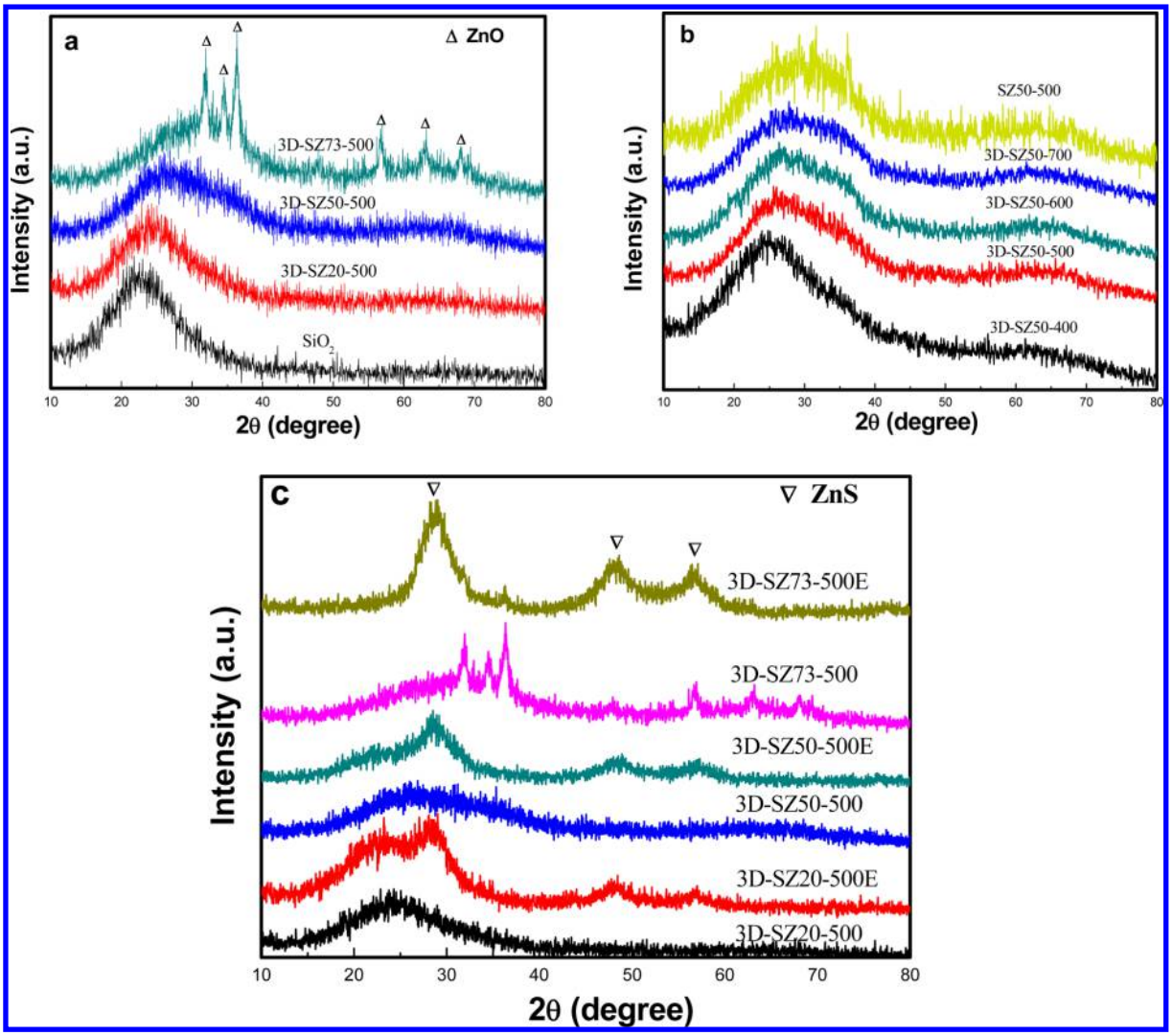

Figure 3. XRD patterns of fresh samples (a, b) and sulfided samples (c).

gradually. In addition, the shoulder and band of SZ50-500 are stronger than those of 3D-SZ50-y samples, indicating that the nanoparticles of ZnO in 3D-SZ50-y were smaller than those in SZ50-500 samples. It has been proved that the silica−zinc oxide complex can improve the dispersion of ZnO and control the nanoparticle size distribution by restraining the movement and aggregation of ZnO particles.[39,41] The above results further confirm that the structure of 3DOM had the similar effect.

After the adsorption of hydrogen sulfide, clear and intense reflection peaks assigned to the ZnS phase appeared in the patterns of the sulfided samples (Figure 3c), indicating that the product of H_2S sorption over the materials was ZnS.

3.3. FTIR Analysis. FTIR spectra of SiO_2 and 3D-SZ50-500 composites before and after desulfurization are shown in Figure 4. There are four adsorption bands at 461, 795, 1080 and 1210 cm^{-1}, which are the characteristic peaks of silica due to backbone vibrations of Si−O−Si.[42,43] And this is associated with the formation of a condensed silica network. The peak at 960 cm^{-1} is characteristic of the Si−OH stretching modes,[41] whereas the two adsorption peaks at 1633 and 3433 cm^{-1} are assigned respectively to the H−OH bending vibration of adsorbed H_2O and the O−H asymmetrical stretching vibration of structural water. Those bands at 2843, 2919 and 2985 cm^{-1} correspond to stretching and deformation vibrations of C−H.[44]

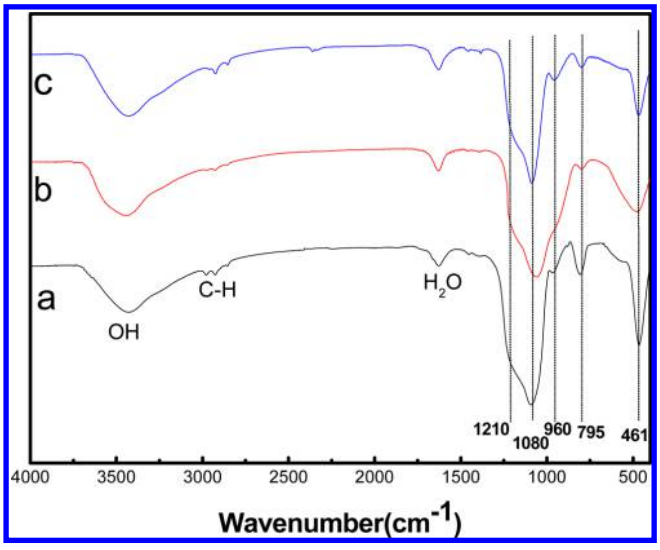

Figure 4. FTIR spectra of SiO_2 (a), 3D-SZ50−500 samples before (b) and after (c) desulfurization.

In the FTIR spectra of the 3D-SZ50-500 sample (Figure 4b), it can be seen that the peak at 461 cm^{-1} becomes broader

dx.doi.org/10.1021/am506077j | ACS Appl. Mater. Interfaces 2014, 6, 21167−21177

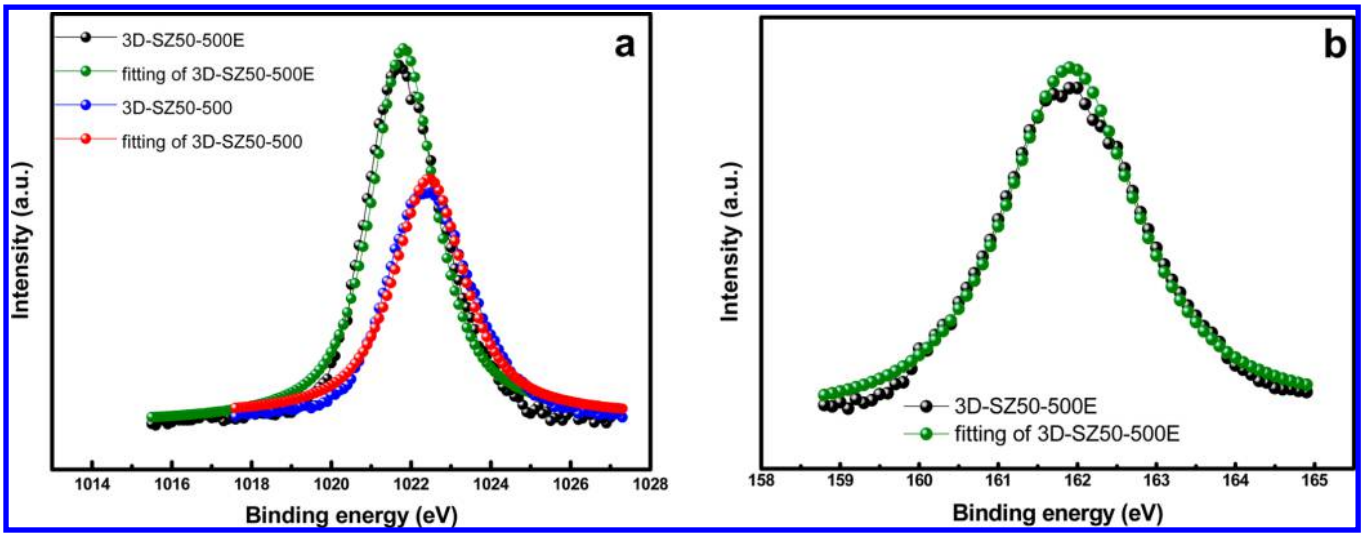

Figure 5. XPS spectra of Zn $2p_{3/2}$ (a) and S 2p (b) narrow spectra for 3D-SZ50-500 samples before and after desulfurization.

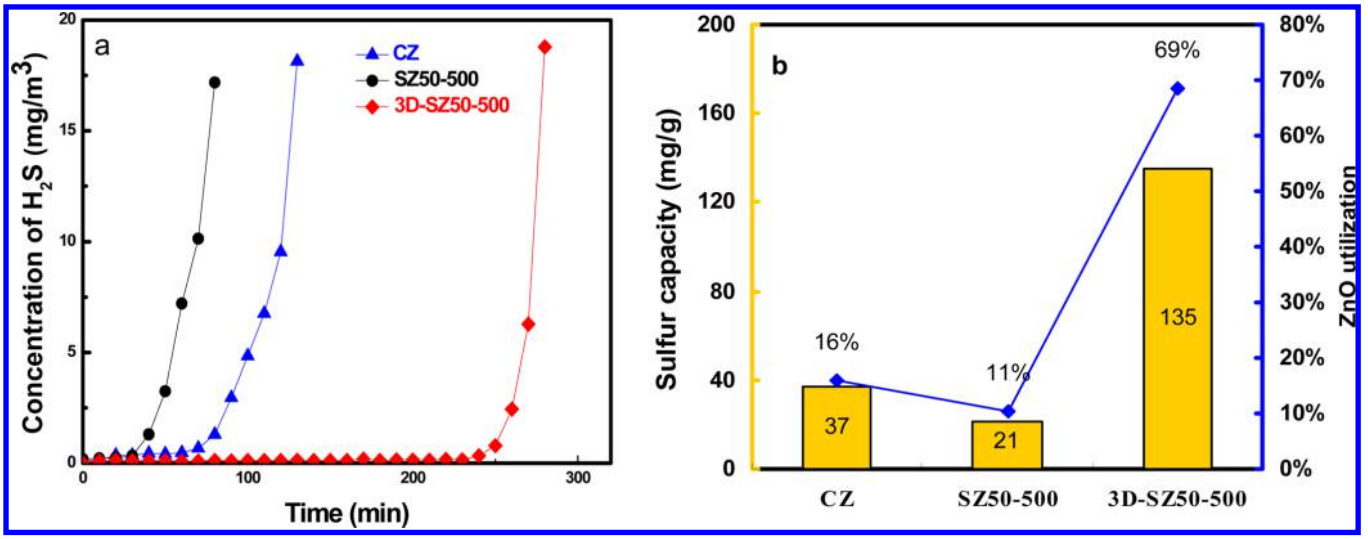

Figure 6. H_2S breakthrough curves for CZ, SZ50-500, 3D-SZ50-500 (a) and the corresponding breakthrough sulfur capacities and ZnO utilization levels (b).

compared to that of the SiO_2, which is attributed to the introduction of ZnO. Because this peak is also corresponding to the characteristic peaks of ZnO and overlapped with O−Si−O.[45] While the intensity of the peak at 960 cm^{-1} is weakened obviously, indicating the well dispersion of ZnO in silica-zinc oxide composites. From Figure 4c, it can be observed that the peak at 461 cm^{-1} declined after the desulfurization process while the peak at 960 cm^{-1} increased; it is worth noting that the peak assigned to Si−OH is overlapped with that of ZnS.[45] So, it can be considered that ZnO is converted to ZnS by reaction with hydrogen sulfide.

3.4. XPS Analysis. Figure 5 shows the XPS spectra of Zn $2p_{3/2}$ and S 2p for 3D-SZ50-500 before and after desulfurization. As can be seen from high-resolution XPS curves in the region of 1020−1025 eV in Figure 5a, there is a single normal peak at a binding energy of 1022.4 eV. This peak is assigned to a characteristic of ZnO.[18,46] After desulfurization, the BE of Zn $2p_{3/2}$ shifts from 1022.4 to 1021.8 eV, indicating that ZnO converted to ZnS after interaction with H_2S.[24,47] In Figure 5b, one normal peak of S 2p was observed at 161.8 eV, which is assigned the S^{2-} in Zn−S.[46,48] No other zinc or sulfur species were found.

3.5. Desulfurization Performance. *3.5.1. H_2S Breakthrough Capacities of 3D-SZ50-500 versus SZ50-500 and Commercial Adsorbents.* The prepared 3D-SZ50-500 sorbent was evaluated for removal of H_2S at room temperature (30 °C) in the presence of ca. 3% moisture, in comparison with that of the commercial sorbent and the SZ50-500 sorbent under the same conditions. H_2S breakthrough curves for the three adsorbents are shown in Figure 6a, and the corresponding breakthrough capacities as well as ZnO utilization levels are presented in Figure 6b. To make clear the contribution of physisorption of H_2S on the material, H_2S breakthrough curve of 3D-SiO_2, with surface area of 245 m^2/g (see Figures S4 and S5 and Table S1, Supporting Information), was measured as well at the same conditions mentioned above. The results show that saturation of the 3D-SiO_2 bed was completed in only 3 min. This indicates that physisorption of H_2S can be negligible, and the sulfur capacity is due to the reactive adsorption resulted from the reaction between ZnO and H_2S. Figure 6a shows that the H_2S concentration in the outlet could be effectively

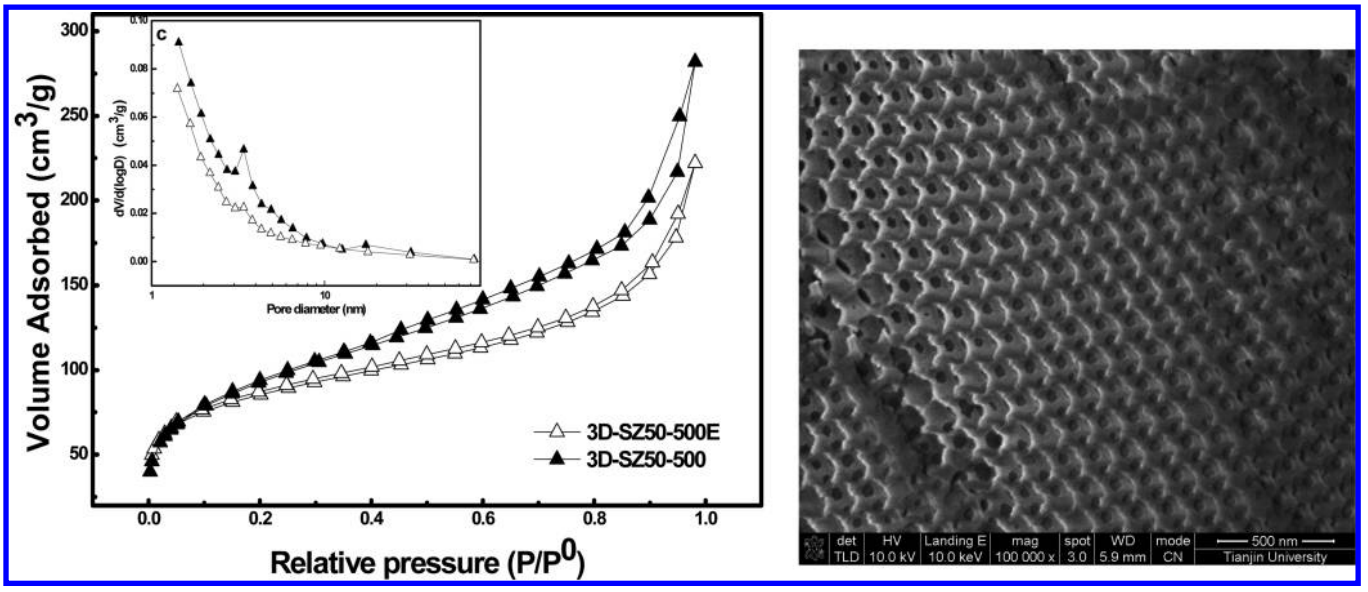

Figure 7. Nitrogen adsorption−desorption isotherms of 3D-SZ50-500 sample before and after desulfurization (inset: PSDs calculated by BJH method) and SEM image of 3D-SZ50-500 sample after desulfrization.

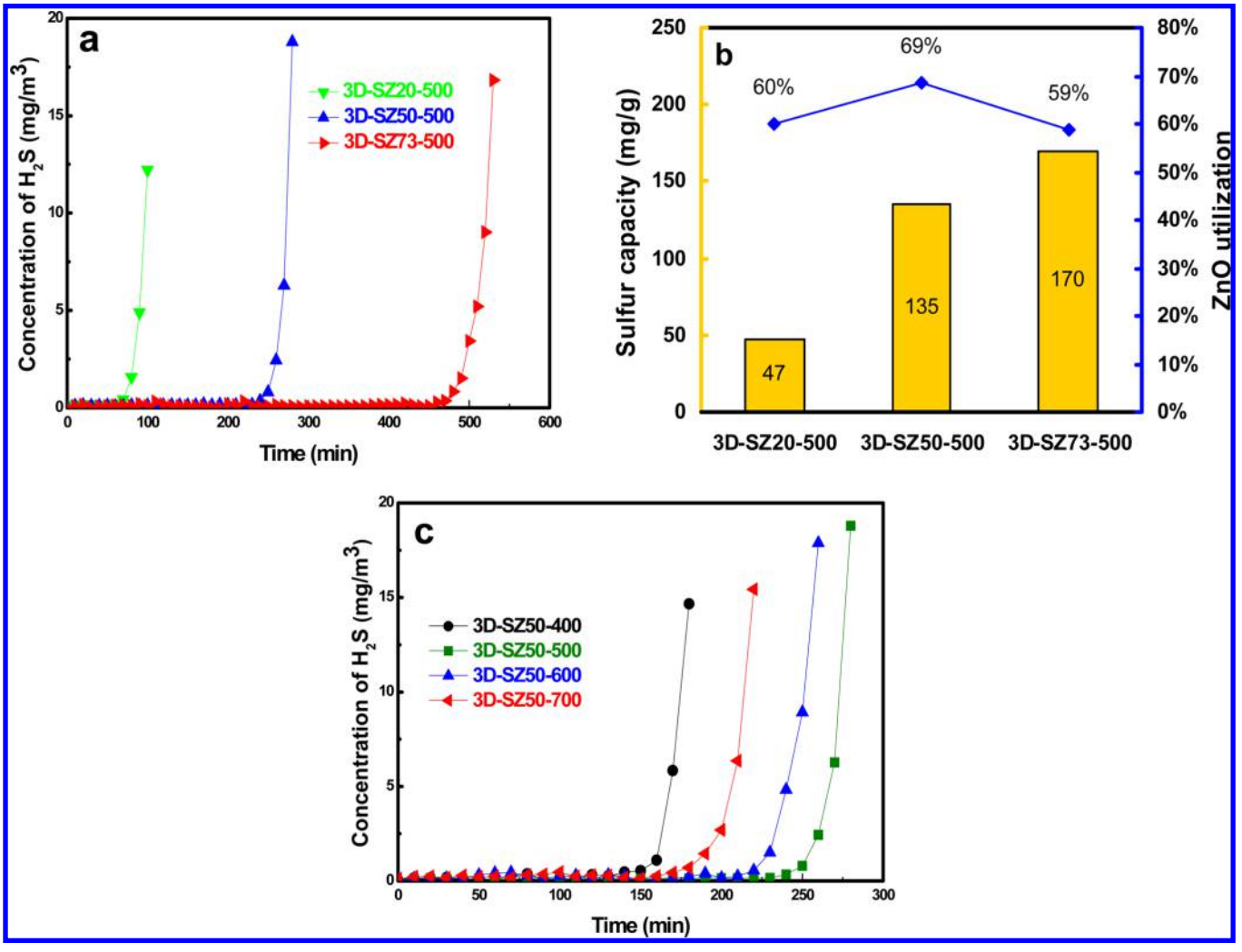

Figure 8. H_2S breakthrough curves for 3D-SZx-500 samples treated at 500 °C with different ZnO content (a), 3D-SZ50-y samples treated at different temperature with 50 wt % ZnO (c) and breakthrough sulfur capacities and ZnO utilization levels of 3D-SZx-500 samples (b).

dx.doi.org/10.1021/am506077j | ACS Appl. Mater. Interfaces 2014, 6, 21167−21177

Table 2. Comparison of Sulfur Capacities of ZnO-based Sorbents Cited in the Literature

sorbent	inlet H_2S (mg/m^3)	outlet H_2S (mg/m^3)	T (°C)	sulfur capacity (mg S/g sorbent)	reference
ZnO/SiO_2	150	<1.5	20	90.7	18
Zn-40-Co-60	1500	<150	room temperature	214.6	17
ZnGO-20	1500	<150	room temperature	146	49
$Cu\text{-}ZnO/SiO_2$	15000	<15000	room temperature	77	50
Fe-Mn-Zn-Ti-O	900	<900	25	80	16
3D-SZ73-500	500	<1	30	170	this work

maintained at <1 mg/m^3 before breakthrough. However, remarkable differences in breakthrough capacity and in ZnO utilization were found (Figure 6b). Sorbent 3D-SZ50-500 was much better than the commercial sorbent CZ, as its breakthrough capacity (135 mg/g) and its ZnO utilization (69%) were higher, despite that the latter contained a greater amount of the active component, ZnO. SZ50-500, which has the same composition as that of 3D-SZ50-500 but lacks a 3DOM structure, had the lowest desulfurization performance, as its breakthrough capacity was only 21 mg/g, similar to the performance noted by Liu et al.[18]

As mentioned before, nanosized grains can enhance the reactivity with H_2S at low temperature and high surface areas can provide more active sites. Both properties are very beneficial for improving the desulfurization performance. In our work, sorbent SZ-50-500 had a considerably large surface area (216 m^2/g), which was almost 3.6 times that of CZ (Table S1, Supporting Information). Moreover, the crystal size of SZ-50-500 was smaller than that of CZ, as determined by XRD (Figure S3, Supporting Information). However, its actual sulfur capacity was far lower than that of the latter. Such a big difference cannot simply be attributed to the high ZnO content of CZ, which is evidenced by the identical compositions of 3D-SZ50-500 and SZ-50-500. It suggests that differences in pore structure mainly resulted in the different results.

Desulfurization of a sulfur compound by metal oxides is a process of volume expansion. The sorbent becomes more and more compact and pore closure even occurs in some severe cases during the reaction.[33] This prevents gaseous reactive molecules from reaching the interior fresh active sites, leading to a very low uptake and utilization of sorbent, especially at ambient temperature. 3DOM sorbents have larger surface areas and smaller nanocrystals and are hierarchically porous. More importantly, they have well-ordered, interconnected, three-dimensional macropores. Compared with that in microporous or mesoporous materials, mass transport in 3DOM materials is relatively efficient, and their surface is highly accessible because the high degree of pore interconnectedness in the three-dimensional structure provides transport paths with little tortuosity. Additionally, macropores can significantly relieve the effect of pore blocking during sulfidation. This ability explains why 3DOM sorbents exhibit desulfurization performance higher than that of SZ-50-500, which possesses mesopores only (Figure S4, Supporting Information). That is, the high performance of 3D-SZ50-500 is attributed to the unique features of 3DOM sorbents.

It is of interest to obtain information on structural changes in 3DOM sorbents after sulfur absorption. To examine such changes, spent 3D-SZ50-500 was subjected to SEM and nitrogen adsorption characterization. The SEM image in Figure 7 shows that the well-ordered, three-dimensional macroporous structure of the spent sample was intact but become denser. Comparative results of nitrogen adsorption measurements show that the spent sample produced a similar isotherm to that of the fresh sample. However, the volume of adsorbed nitrogen decreased markedly, indicating that although the overall porous structure was intact, numerous pores were blocked, especially pores with sizes within 3−4 nm and 10−30 nm (see inset of Figure 7). BET surface areas were also reduced from 336 to 174 m^2/g (Table 1). These results are in good agreement with the aforementioned results.

3.5.2. Effects of Zn/Si Ratio and Calcination Temperature of 3DOM Composites on the Desulfurization Performance. To optimize the formula of 3D-SZ adsorbents for desulfurization, the effect of Zn/Si ratio and calcination temperature for the 3DOM composites on the desulfurization performance were studied at room temperature (30 °C) in the presence of ca. 3% moisture (results are shown in Figure 8). Figure 8a illustrates that with the increase in ZnO content from 20% to 73%, the breakthrough time increased sharply, and the breakthrough capacity increased from 47 to 170 mg/g (Figure 8b) which is 4.5 times that of the commercial sorbent and superior to those of most of other ZnO-based sorbents available in the literature (shown in Table 2). However, the degree of ZnO utilization first increased and then decreased. This is because that 3D-SZx-500 sorbents are composites of silica and zinc oxide; the presence of silica in the sorbent benefits the dispersion of zinc oxide and therefore improves the desulfurization performance. However, greater silica content can result in zinc oxide covered to some extent, which hampers contact of zinc oxide with reactive gas.[18] On the contrary, when the ZnO content increases excessively, silica cannot efficiently reduce ZnO aggregation, resulting in a reduction of the active sites. This explains why utilization is low when the ZnO content is too high or too low.

Figure 8c shows that as the temperature increased, the breakthrough time first increased and reached a maximum value at 500 °C and then decreased. Residual amounts of carbon impurities were present in 3D-SZ50-400 due to insufficient calcination. These carbon impurities could cover the surface of ZnO and partially block the pore channels, thus decreasing the sulfur capacity. However, when the calcination temperature was >500 °C, the channels gradually shrank, and the surface area and pore volume decreased, as revealed by nitrogen adsorption data. In addition, XRD results (Figure 3) illustrate that the grain size increased with the increase in calcination temperature. Together, the above results suggest a reduction of sulfur capacity of 3D-SZ50-600 and 3D-SZ50-700.

3.5.3. Effect of Moisture and Sorption Temperature on the Desulfurization Performance. The influence of moisture on H_2S capture was investigated by using the 3D-SZ50-500 sample. Breakthrough experiments were carried out at room temperature under wet or dry conditions. The former condition is described in section 2.2 In dry conditions, the sorbent was pretreated for 2 h at 200 °C under nitrogen flow to remove adsorbed water and dry N_2 containing 500 mg/m^3 H_2S was

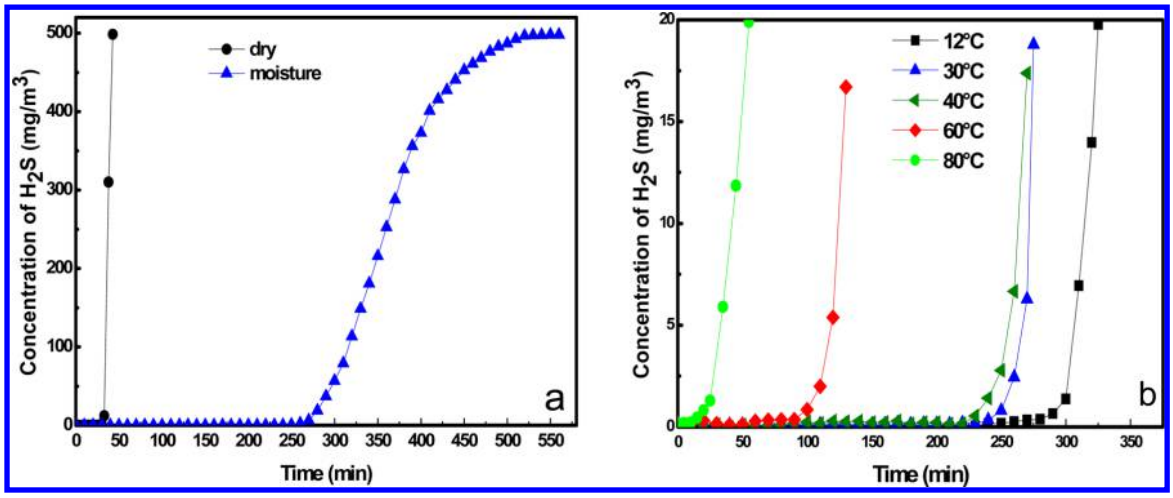

Figure 9. H_2S breakthrough curves for 3D-SZ50-500 under dry/moisture condition (a) and at different sorption temperature (b).

then introduced into the bed. Results shown in Figure 9a illustrate that 3D-SZ50-500 had very poor activity for sulfur capture under dry conditions. Breakthrough of the sorbent bed was completed very early, and the balance of H_2S between the inlet and outlet was reached in only 30 min at very low breakthrough capacity (16 mg/g). In contrast to the above result, 3D-SZ50-500 showed high performance in H_2S sorption in the presence of moisture. The breakthrough time increased to 250 min, and the corresponding capacity increased to 135 mg/g, almost 8.4 times that in dry atmosphere. ZnO utilization degree of the sorbent reached 69%. Evidently, the presence of moisture markedly enhanced H_2S sorption by the 3D-SZ composites. To understand the influence of water vapor on H_2S sorption, another experiment in the presence of moisture was conducted at different absorption temperatures. As shown in Figure 9b, the breakthrough time of 3D-SZ50-500 decreased markedly with the increase in sorption temperature.

The above results indicate that water vapor exerts its influence mainly by condensing as a film on the ZnO surface. First, H_2S can be absorbed by the water film.[51] Furthermore, hydroxylation occurs on the surface of ZnO in contact with the liquid water film, which in turn leads to gradual alkalinification of the water film.[52,53] Basic conditions can trigger the dissociation of dissolved H_2S into $HS^-$and S^{2-}.[15,54,55] At higher temperatures, the liquid water film thins and even disappears, thereby decreasing the absorption and dissociation of H_2S.[52] Therefore, desulfurization reaction over our material in the presence of water at room temperature follows the process:

$$ZnO + H_2O \rightarrow Zn^{2+} + 2OH^-$$

$$H_2S + OH^- \rightarrow HS^- + H_2O,\ HS^- + OH^- \rightarrow S^{2-} + H_2O$$

$$Zn^{2+} + S^{2-} \rightarrow ZnS$$

3.5.4. Regeneration Performance of the Sorbent. Considering the economic and commercial use of the sorbent, the performance of regeneration was also explored. The regeneration of the sulfided sorbent was performed in a tube furnace with air at a flow rate of 100 mL/min at 500 °C for 4 h. Figure 10 shows the sulfur capacities of the sorbent 3D-SZ50-500 during H_2S adsorption/regeneration cycles. It can be seen that the sorbent exhibited acceptable regenerability and stability.

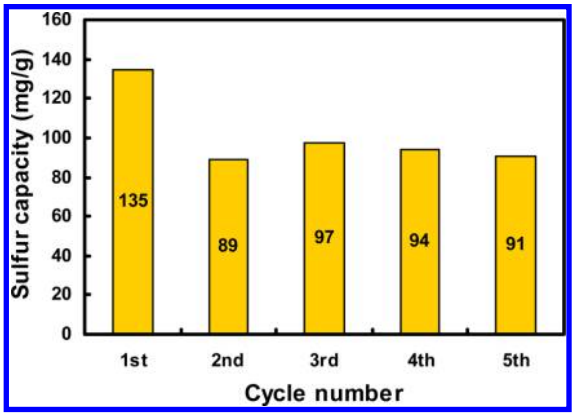

Figure 10. Sulfur capacities of the 3D-SZ50-500 sorbent during adsorption/regeneration cycles.

Even at the fifth cycle, the sulfur capacity still reached 91 mg/g, which is 67.4% of that of the fresh sorbent. The incomplete regeneration is significantly related to the regeneration conditions, such as temperature, atmosphere (oxygen concentration, water vapor) and so on.[56−58] To improve the regeneration performance, further work should be done in the future.

4. CONCLUSIONS

The presented results showed that 3DOM ZnO−SiO_2 composites prepared by colloidal crystal template method had a well-ordered and interconnected pore network with hierarchically porous, high surface areas and nanocrystalline ZnO. These special features of 3DOM composites can strongly enhance reactive adsorption of hydrogen sulfide at ambient temperature. For 3D-SZ-50-500 composites, the H_2S breakthrough capacity and ZnO utilization degree were much higher than those of the commercial ZnO sorbents as well as SZ composites without 3DOM. The ZnO content in 3DOM composites and calcination temperature of 3DOM composites had great influences on the structure of 3DOM and the desulfurization performance. Moisture in the gas phase has a positive effect on the process of H_2S removal. In addition, the results of multiple H_2S adsorption/regeneration cycles indicated that the 3D-SZ sorbent can be used after regeneration. After 4 times regeneration, the sulfur capacity can still reach 67.4% of the

first value. It is considered that the novel 3DOM ZnO−SiO_2 composites may be a promising sorbents for H_2S removal at ambient temperature.

■ ASSOCIATED CONTENT

Supporting Information

SEM images of PS colloidal crystal template, 3D-SZ50-400, 3D-SZ50-600, 3D-SZ50-700, XRD patterns of SZ50-500 and CZ, nitrogen adsorption−desorption isotherms of 3D-SiO_2 and SZ50-500, breakthrough curve for 3D-SiO_2 and texture parameters of 3D-SiO_2, SZ50-500 and CZ. This material is available free of charge via the Internet at http://pubs.acs.org.

■ AUTHOR INFORMATION

Corresponding Author

*H.-L. Fan. Tel.: 0086-351-6010530. E-mail: fanhuiling@tyut.edu.cn.

Notes

The authors declare no competing financial interest.

■ ACKNOWLEDGMENTS

This work was financially supported by National Cooperation Project of Shanxi Province (2014081007-3) and National Nature Science Fundamental (21276172). Additional support was provided by Scientific Research Foundation for Returned Scholars, Ministry of Education of China. We deeply appreciate Mr. Zhen Tian for very useful discussion about nitrogen adsorption results.

■ REFERENCES

(1) Stirling, D. *The Sulfur Problem: Cleaning up Industrial Feedstocks*; RSC Clean Technology Monographs; Royal Society of Chemistry: Cambridge, U.K., 2000; Chapter 3, pp 16−29.

(2) Eslek Koyuncu, D. D.; Yasyerli, S. Selectivity and Stability Enhancement of Iron Oxide Catalyst by Ceria Incorporation for Selective Oxidation of H_2S to Sulfur. *Ind. Eng. Chem. Res.* **2009**, *48*, 5223−5229.

(3) Belmabkhout, Y.; Weireld, G. D.; Sayari, A. Amine-Bearing Mesoporous Silica for CO_2 and H_2S Removal from Natural Gas and Biogas. *Langmuir* **2009**, *25*, 13275−13278.

(4) Polychronopoulou, K.; Fierro, J. L. G.; Efstathiou, A. M. Novel Zn−Ti-based Mixed Metal Oxides for Low-Temperature Adsorption of H_2S from Industrial Gas Streams. *Appl. Catal., B* **2005**, *57*, 125−137.

(5) Rezaei, S.; Tavana, A.; Sawada, J. A.; Wu, L.; Junaid, A. S.M.; Kuznicki, S. M. Novel Copper-Exchanged Titanosilicate Adsorbent for Low Temperature H_2S Removal. *Ind. Eng. Chem. Res.* **2012**, *51*, 12430−12434.

(6) Dhage, P.; Samokhvalov, A.; Repala, D.; Duin, E. C.; Tatarchuk, B. J. Regenerable Fe−Mn−ZnO/SiO_2 Sorbents for Room Temperature Removal of H_2S from Fuel Reformates: Performance, Active Sites, Operando Studies. *Phys. Chem. Chem. Phys.* **2011**, *13*, 2179−2187.

(7) Li, L. Y.; King, D. L. H_2S Removal with ZnO during Fuel Processing for PEM Fuel Cell Applications. *Catal. Today* **2006**, *116*, 537−541.

(8) Novochinskii, I. I.; Song, C.; Ma, X.; Liu, X.; Shore, L.; Lampert, J.; Farrauto, R. J. Low-Temperature H_2S Removal from Steam-Containing Gas Mixtures with ZnO for Fuel Cell Application. 1. ZnO Particles and Extrudates. *Energy Fuels* **2004**, *18*, 576−583.

(9) Ros, A.; Montes-Moran, M. A.; Fuente, E.; Nevskaia, D. M.; Martin, M. J. Dried Sludges and Sludge-Based Chars for H_2S Removal at Low Temperature: Influence of Sewage Sludge Characteristics. *Environ. Sci. Technol.* **2006**, *40*, 302−309.

(10) Garces, H. F.; Espinal, A. E.; Suib, S. L. Tunable Shape Microwave Synthesis of Zinc Oxide Nanospheres and Their Desulfurization Performance Compared with Nanorods and Platelet-like Morphologies for the Removal of Hydrogen Sulfide. *J. Phys. Chem. C* **2012**, *116*, 8465−8474.

(11) Garces, H. F.; Galindo, H. M.; Garces, L. J.; Hunt, J.; Morey, A.; Suib, S. L. Low Temperature H_2S Dry-Desulfurization with Zinc Oxide. *Microporous Mesoporous Mater.* **2010**, *127*, 190−197.

(12) Sun, J.; Modi, S.; Liu, K.; Lesieur, R.; Buglass, J. Kinetics of Zinc Oxide Sulfidation for Packed-Bed Desulfurizer Modeling. *Energy Fuels* **2007**, *21*, 1863−1871.

(13) Samokhvalov, A.; Tatarchuk, B. J. Characterization of Active Sites, Determination of Mechanisms of H_2S, COS and CS_2 Sorption and Regeneration of ZnO Low-Temperature Sorbents: Past, Current and Perspectives. *Phys. Chem. Chem. Phys.* **2011**, *13*, 3197−3209.

(14) Huang, Z.-H.; Liu, G.; Kang, F. Glucose-Promoted Zn-based Metal−Organic Framework/Graphene Oxide Composites for Hydrogen Sulfide Removal. *ACS Appl. Mater. Interfaces* **2012**, *4*, 4942−4947.

(15) Seredych, M.; Mabayoje, O.; Bandosz, T. J. Visible-Light-Enhanced Interactions of Hydrogen Sulfide with Composites of Zinc (Oxy) Hydroxide with Graphite Oxide and Graphene. *Langmuir* **2012**, *28*, 1337−1346.

(16) Polychronopoulou, K.; Efstathiou, A. M. Effects of Sol-Gel Synthesis on 5Fe-15Mn-40Zn-40Ti-O Mixed Oxide Structure and its H_2S Removal Efficiency from Industrial Gas Streams. *Environ. Sci. Technol.* **2009**, *43*, 4367−4372.

(17) Mabayoje, O.; Seredych, B.; Bandosz, T. J. Enhanced Adsorption of Hydrogen Sulfide on Mixed Zinc/Cobalt Hydroxides: Effect of Morphology and an Increased Number of Surface Hydroxyl Groups. *Colloid Interface Sci.* **2013**, *405*, 218−225.

(18) Liu, G.; Huang, Z.-H.; Kang, F. Preparation of ZnO/SiO_2 Gel Composites and Their Performance of H_2S Removal at Room Temperature. *J. Hazard. Mater.* **2012**, *215*, 166−172.

(19) Montes, D.; Tocuyo, E.; González, E.; Rodríguez, D.; Solano, R.; Atencio, R.; Ramos, M. A.; Moronta, A. Reactive H_2S Chemisorption on Mesoporous Silica Molecular Sieve-Supported CuO or ZnO. *Microporous Mesoporous Mater.* **2013**, *168*, 111−120.

(20) Baird, T.; Denny, P. J.; Hoyle, R. W.; McMonagle, F.; Stirling, D.; Tweedy, J. Modified Zinc-Oxide Absorbents for Low-Temperature Gas Desulfurization. *J. Chem. Soc. Faraday Trans.* **1992**, *88*, 3375−3382.

(21) Baird, T.; Campbell, K. C.; Holliman, P. J.; Hoyle, R. W.; Huxam, M.; Stirling, D.; Williams, B. P.; Morris, M. Cobalt-Zinc Oxide Absorbents for Low Temperature Gas Desulfurisation. *J. Mater. Chem.* **1999**, *9*, 599−605.

(22) Carnes, C. L.; Klabunde, K. Unique Chemical Reactivities of Nanocrystalline Metal Oxides toward Hydrogen Sulfide. *J. Chem. Mater.* **2002**, *14*, 1806−1811.

(23) Hussain, M.; Abbas, N.; Fino, D.; Russo, N. Novel Mesoporous Silica Supported ZnO Adsorbents for the Desulphurization of Biogas at Low Temperatures. *Chem. Eng. J.* **2012**, *188*, 222−232.

(24) Hernández, S. P.; Chiappero, M.; Russo, N.; Fino, D. A Novel ZnO-based Adsorbent for Biogas Purification in H_2 Production Systems. *Chem. Eng. J.* **2011**, *176*, 272−279.

(25) Davidson, J. M.; Lawrie, C. H.; Sohail, K. Kinetics of the Absorption of Hydrogen Sulfide by High Purity and Doped High Surface Area Zinc Oxide. *Ind. Eng. Chem. Res.* **1995**, *34*, 2981−2989.

(26) Davidson, J. M.; Grant, C. M.; Winpenny, R. E. P. Fast Reaction of Solid Copper(I) Complexes with Hydrogen Sulfide Gas. *Ind. Eng. Chem. Res.* **2001**, *40*, 2982−2986.

(27) Davidson, J. M.; Glass, D. H. Nucleation Kinetics in the Reactions of Nickel Basic Carbonates with Hydrogen Sulfide: The Carbonate Precipitation Reactions of Divalent Nickel. *Ind. Eng. Chem. Res.* **2007**, *46*, 4772−4777.

(28) Rosso, I.; Galletti, C.; Bizzi, M.; Saracco, G.; Specchia, V. Zinc Oxide Sorbents for the Removal of Hydrogen Sulfide from Syngas. *Ind. Eng. Chem. Res.* **2003**, *42*, 1688−1697.

(29) Cai, S.; Zhang, D.; Zhang, L.; Huang, L.; Li, H.; Gao, R.; Shi, L.; Zhang, J. Comparative Study of 3D Ordered Macroporous

$Ce_{0.75}Zr_{0.2}M_{0.05}O_2-\delta$ (M = Fe, Cu, Mn, Co) for Selective Catalytic Reduction of NO with NH_3. *Catal. Sci. Technol.* **2014**, *4*, 93−101.
(30) Wei, Y. C.; Liu, J.; Zhao, Z.; Chen, Y. S.; Xu, C. M.; Duan, A. J.; Jiang, G. Y.; He, H. Highly Active Catalysts of Gold Nanoparticles Supported on Three Dimensionally Ordered Macroporous $LaFeO_3$ for Soot Oxidation. *Angew. Chem., Int. Ed.* **2011**, *50*, 2326−2329.
(31) Stein, A.; Wilson, B. E.; Rudisill, S. G. Design and Functionality of Colloidal-Crystal-Templated Materials—Chemical Applications of Inverse Opals. *Chem. Soc. Rev.* **2013**, *42*, 2763−2803.
(32) Stein, A.; Li, F.; Denny, N. R. Morphological Control in Colloidal Crystal Templating of Inverse Opals, Hierarchical Structures, and Shaped Particles. *Chem. Mater.* **2008**, *20*, 649−666.
(33) Fan, H. L.; Sun, T.; Zhao, Y. P.; Shangguan, J.; Lin, J. Y. Three-Dimensionally Ordered Macroporous Iron Oxide for Removal of H_2S at Medium Temperatures. *Environ. Sci. Technol.* **2013**, *47*, 4859−4865.
(34) Liu, Y.; Liu, B. C.; Wang, Q.; Liu, Y. X.; Li, C. Y.; Hu, W. T.; Jing, P.; Zhao, W. Z.; Zhang, J. Three Dimensionally Ordered Macroporous Au/CeO_2 Catalysts Synthesized via Different Methods for Enhanced CO Preferential Oxidation in H_2-rich Gases. *RSC Adv.* **2014**, *4*, 5975−5985.
(35) Davis, M.; Ramirez, D. A.; Hope-Weeks, L. J. Formation of Three-Dimensional Ordered Hierarchically Porous Metal Oxides via a Hybridized Epoxide Assisted/Colloidal Crystal Templating Approach. *ACS Appl. Mater. Interfaces* **2013**, *5*, 7786−7792.
(36) Wei, Y. C.; Zhao, Z.; Li, T.; Liu, J.; Duan, A. J.; Jiang, G. Y. The Novel Catalysts of Truncated Polyhedron Pt Nanoparticles Supported on Three-Dimensionally Ordered Macroporous Oxides (Mn, Fe, Co, Ni, Cu) with Nanoporous Walls for Soot Combustion. *Appl. Catal., B* **2014**, *146*, 57−70.
(37) Li, W.-C.; Lu, A.-H.; Weidenthaler, C.; Schüth, F. Hard-Templating Pathway To Create Mesoporous Magnesium Oxide. *Chem. Mater.* **2004**, *16*, 5676−5681.
(38) Dionig, C.; Calestani, G.; Ferraroni, T.; Ruani, G.; Liotta, L. F.; Migliori, A.; Nozar, P.; Palles, Dimitros. Template Evaporation Method for Controlling Anatase Nanocrystal Size in Ordered Macroporous TiO_2. *J. Colloid Interface Sci.* **2005**, *290*, 201−207.
(39) Cannas, C.; Casu, M.; Lai, A.; Musinu, A.; Piccaluga, G. XRD, TEM and ^{29}Si MAS NMR Study of Sol−Gel $ZnO-SiO_2$ Nanocomposites. *J. Mater. Chem.* **1999**, *9*, 1765−1769.
(40) Mureddu, M.; Ferino, I.; Rombi, E.; Cutrufello, M. G.; Deiana, P.; Ardu, A.; Musinu, A.; Piccaluga, G.; Cannas, C. ZnO/SBA-15 Composites for Mid-Temperature Removal of H_2S: Synthesis, Performance and Regeneration Studies. *Fuel* **2012**, *102*, 691−700.
(41) Firmansyah, D. A.; Kim, S.-G.; Lee, K.-S.; Zahaf, R.; Kim, Y. H.; Lee, D. Microstructure-Controlled Aerosol−Gel Synthesis of ZnO Quantum Dots Dispersed in SiO_2 Nanospheres. *Langmuir* **2012**, *28*, 2890−2896.
(42) Yang, H. M.; Xiao, Y.; Liu, K.; Feng, Q. M. Chemical Precipitation Synthesis and Optical Properties of ZnO/SiO_2 Nanocomposites. *J. Am. Ceram. Soc.* **2008**, *91*, 1591−1596.
(43) Rubio, F.; Rubio, J.; Oteo, J. L. A FT-IR Study of the Hydrolysis of Tetraethylorthosilicate (TEOS). *Spectrosc. Lett.* **1998**, *31*, 199−219.
(44) Estella, J.; Echeverría, J. C.; Laguna, M.; Garrido, J. J. Effects of Aging and Drying Conditions on The Structural and Textural Properties of Silica Gels. *Microporous Mesoporous Mater.* **2007**, *102*, 274−282.
(45) Wang, X.; Jia, J.; Zhao, L.; Sun, T. Chemisorption of Hydrogen Sulphide on Zinc Oxide Modified Aluminum-Substituted SBA-15. *Appl. Surf. Sci.* **2008**, *254*, 5445−5451.
(46) Wang, X. H.; Sun, T. H.; Yang, J.; Zhao, L.; Jia, J. P. Low-Temperature H_2S Removal from Gas Streams with SBA-15 Supported ZnO Nanoparticles. *Chem. Eng. J.* **2008**, *142*, 48−55.
(47) Rodriguez, J. A.; Jirsak, T.; Chaturvedi, S.; Hrbek, J. The Interaction of H_2S and S_2 with Cs and Cs/ZnO Surfaces: Photoemission and Molecular-Orbital Studies. *Surf. Sci.* **1998**, *407*, 171−188.
(48) Liu, L.; Xie, R.; Yang, L.; Xiao, D.; Zhu, J. Synthesis, Structural, and Optical Properties of Core/Shell ZnS:Fe/ZnS Nanocrystals. *Phys. Status Solidi A* **2011**, *208*, 863−867.
(49) Mabayojea, O.; Seredych, M.; Bandosz, T. J. Reactive Adsorption of Hydrogen Sulfide on Visible Light Photoactive Zinc (hydr)oxide/Graphite Oxide and Zinc (hydr)oxychloride/Graphite Oxide Composites. *Appl. Catal., B* **2013**, *132*, 321−331.
(50) Dhage, P.; Samokhvalov, A.; Repala, D.; Duin, E. C.; Bowman, M.; Tatarchuk, B. J. Copper-Promoted ZnO/SiO_2 Regenerable Sorbents for the Room Temperature Removal of H_2S from Reformate Gas Streams. *Ind. Eng. Chem. Res.* **2010**, *49*, 8388−8396.
(51) He, R.; Xia, F.-F.; Wang, J.; Pan, C.-L.; Fang, C.-R. Characterization of Adsorption Removal of Hydrogen Sulfide by Waste Biocover Soil, an Alternative Landfill Cover. *J. Hazard. Mater.* **2011**, *186*, 773−778.
(52) Noei, H.; Qiu, H.; Wang, Y.; Löffler, E.; Wöll, C.; Muhler, M. The Identification of Hydroxyl Groups on ZnO Nanoparticles by Infrared Spectroscopy. *Phys. Chem. Chem. Phys.* **2008**, *10*, 7092−7097.
(53) Raymand, D.; van Duin, A. C. T.; Goddard, W. A., III; Hermansson, K.; Spångberg, D. Hydroxylation Structure and Proton Transfer Reactivity at the Zinc Oxide Water Interface. *J. Phys. Chem. C* **2011**, *115*, 8573−8579.
(54) Mabayoje, O.; Seredych, M.; Bandosz, T. J. Enhanced Reactive Adsorption of Hydrogen Sulfide on the Composites of Graphene/Graphite Oxide with Copper (Hydr)oxychlorides. *ACS Appl. Mater. Interfaces* **2012**, *4*, 3316−3324.
(55) Montes-Morán, M. A.; Concheso, A.; Canals-Batlle, C.; Aguirre, N. V.; Ania, C. O.; Martín, M. J.; Masaguer, V. Linz-Donawitz Steel Slag for the Removal of Hydrogen Sulfide at Room Temperature. *Environ. Sci. Technol.* **2012**, *46*, 8992−8997.
(56) Siriwardane, R. V.; Woodruff, S. In Situ Fourier Transform Infrared Characterization of Sulfur Species Resulting from the Reaction of Water Vapor and Oxygen with Zinc Sulfide. *Ind. Eng. Chem. Res.* **1997**, *36*, 5277−5281.
(57) Song, H. S.; Park, M. G.; Ahn, W.; Lim, S. N.; Yi, K. B.; Croiset, E.; Chen, Z. W.; Nam, S. C. Enhanced Adsorption of Hydrogen Sulfide and Regeneration Ability on The Composites of Zinc Oxide with Reduced Graphite Oxide. *Chem. Eng. J.* **2014**, *253*, 264−273.
(58) Jothimurugesan, K.; Gangwal, S. K. Regeneration of Zinc Titanate H_2S Sorbents. *Ind. Eng. Chem. Res.* **1998**, *37*, 1929−1933.